Cell

LIN28A Is a Suppressor of ER-Associated Translation in Embryonic Stem Cells

Jun Cho,[1,2,4] Hyeshik Chang,[1,2,4] S. Chul Kwon,[1,2] Baekgyu Kim,[1,2] Yoosik Kim,[1,2] Junho Choe,[3] Minju Ha,[1,2] Yoon Ki Kim,[3] and V. Narry Kim[1,2,*]
[1]Institute for Basic Science
[2]School of Biological Sciences
Seoul National University, Seoul 151-742, Korea
[3]School of Life Sciences and Biotechnology, Korea University, Seoul 136-701, Korea
[4]These authors contributed equally to this work
*Correspondence: narrykim@snu.ac.kr
http://dx.doi.org/10.1016/j.cell.2012.10.019

SUMMARY

LIN28 plays a critical role in developmental transition, glucose metabolism, and tumorigenesis. At the molecular level, LIN28 is known to repress maturation of let-7 microRNAs and enhance translation of certain mRNAs. In this study, we obtain a genome-wide view of the molecular function of LIN28A in mouse embryonic stem cells by carrying out RNA crosslinking-immunoprecipitation-sequencing (CLIP-seq) and ribosome footprinting. We find that, in addition to let-7 precursors, LIN28A binds to a large number of spliced mRNAs. LIN28A recognizes AAGNNG, AAGNG, and less frequently UGUG, which are located in the terminal loop of a small hairpin. LIN28A is localized to the periendoplasmic reticulum (ER) area and inhibits translation of mRNAs that are destined for the ER, reducing the synthesis of transmembrane proteins, ER or Golgi lumen proteins, and secretory proteins. Our study suggests a selective regulatory mechanism for ER-associated translation and reveals an unexpected role of LIN28A as a global suppressor of genes in the secretory pathway.

INTRODUCTION

LIN28 is a conserved RNA binding protein whose homologs are found from worms to humans. It was originally identified as a regulator of developmental timing in *Caenorhabditis elegans* (Moss et al., 1997), and its expression is tightly regulated during animal development (Moss and Tang, 2003). Mammals have two homologs, *Lin28a* and *Lin28b*. *Lin28a* is highly expressed in embryonic stem cells (ESCs) and was shown as one of the four factors that convert fibroblasts into induced pluripotent stem cells (Yu et al., 2007). Perturbation of *Lin28* results in developmental defects and tumorigenesis. In mouse, for instance, *Lin28a* deficiency caused undergrowth and lethality in early stages of development, whereas its ectopic expression induced overgrowth and delayed the timing of puberty (Zhu et al., 2010). Furthermore, *Lin28a/b* promote malignant transformation, and their expression is associated with advanced stages of many types of tumors, including hepatocarcinoma, nephroblastoma, ovarian carcinoma, and germ cell tumors (Thornton and Gregory, 2012; Viswanathan et al., 2009).

At the molecular level, LIN28 acts as a suppressor of let-7 microRNA biogenesis (Heo et al., 2008; Newman et al., 2008; Rybak et al., 2008; Viswanathan et al., 2008). In the nucleus, LIN28 binds to the primary transcript of let-7 (pri-let-7) and prevents its processing by RNase III DROSHA (Newman et al., 2008; Viswanathan et al., 2008). In the cytoplasm, it interacts with the precursor form of let-7 (pre-let-7) and interferes with pre-let-7 processing (Heo et al., 2008; Rybak et al., 2008). LIN28 recruits TUTase 4 (ZCCHC11) to induce oligo-uridylation of pre-let-7, which effectively blocks DICER processing and facilitates degradation of the RNA (Hagan et al., 2009; Heo et al., 2008; Heo et al., 2009). Although LIN28B is localized mainly in the nucleolus and interferes with nuclear processing, LIN28A is found mostly in the cytoplasmic compartment and acts in concert with TUTase 4 (Piskounova et al., 2011). LIN28 homologs commonly have two types of RNA binding domains: a cold shock domain and a cluster of two CCHC-type zinc finger motifs. We previously showed by biochemical analyses that the "GGAG" sequences in the terminal loop of let-7 precursors serve as the binding site for the zinc finger domains that are critical for let-7 regulation (Heo et al., 2009). More recent structural studies revealed the molecular basis of the interaction between LIN28 and the terminal loop of pre-let-7 (Loughlin et al., 2012; Nam et al., 2011).

Although let-7 is certainly a key target of LIN28, multiple lines of evidence support additional functions of LIN28. First, during retinoic-acid-induced neurogliogenesis, *Lin28a* overexpression altered the expression of several transcription factors involved in early embryonic cell fate decision before any increase in let-7 level was detected (Balzer et al., 2010). Second, impaired glucose tolerance and insulin resistance were observed in muscle-specific *Lin28a* knockout mice without significant changes in the let-7 level (Zhu et al., 2011). Third, LIN28A interacts with mRNAs and cosediments with polysome in sucrose gradient centrifugation (Balzer and Moss, 2007). Consistently, several studies reported that LIN28A can bind to and enhance translation of certain mRNAs such as *Igf2* in differentiating

myoblasts and *Oct4* in ESCs (Polesskaya et al., 2007; Qiu et al., 2010; Xu and Huang, 2009; Xu et al., 2009).

In order to obtain a genome-wide view of LIN28A's function, we identified LIN28A-interacting RNAs by using a technique that combines UV crosslinking, immunoprecipitation, and high-throughput sequencing (CLIP-seq, also known as HITS-CLIP) (Chi et al., 2009; Licatalosi et al., 2008). This technique takes advantage of UV irradiation of live cells, which introduces covalent bonds between the bases and amino acids (such as Cys, Lys, Phe, Trp, and Tyr) in close proximity (~1 Å), capturing the physiological state of RNA-protein interaction (Licatalosi and Darnell, 2010; Wagenmakers et al., 1980). Because of the crosslinking, one can use harsh immunoprecipitation conditions to eliminate artificial RNA-protein interactions that commonly occur in cell lysates (Dreyfuss et al., 1984). In addition, sequencing of the coimmunopurified RNA fragments provides a global view of the interacting transcriptome and allows mapping of exact binding sites on target RNAs (Kishore et al., 2011; Licatalosi et al., 2008; Ule et al., 2005; Ule et al., 2003; Zhang and Darnell, 2011).

In this study, we find that LIN28A targets not only the let-7 precursors but also a large number of mRNAs. Analyses of the binding sites reveal general features of LIN28A binding motif. We further discover by ribosome footprinting that LIN28A acts as a suppressor of translation in the endoplasmic reticulum (ER) pathway.

RESULTS

LIN28A CLIP-seq from Mouse Embryonic Stem Cells

To purify the LIN28A-RNA complexes, we irradiated mouse embryonic stem cells (mESCs) with UV light, lysed the cells, treated the lysates with RNase A, and immunoprecipitated the complexes by using antibodies against LIN28A. RNA fragments from the immunoprecipitates were ligated to linkers, amplified by RT-PCR and sequenced with Illumina Genome Analyzer IIx (Figures 1A and S1A available online).

To ensure specific isolation of LIN28A-interacting RNAs, we obtained three different libraries by using three anti-LIN28A antibodies, one rabbit polyclonal antibody (Abcam) and two mouse monoclonal antibodies raised in-house (35L33G and 2J3). The amounts of RNA recovered from immunoprecipitates were significantly reduced when LIN28A was depleted, indicating that the antibodies specifically precipitated the LIN28A protein and its target RNAs (Figures 1B and S1B).

About 32 million reads were obtained from each CLIP cDNA library and 32% of them were confidently mapped to unique positions in the mouse genome (Table S1). To assess the reproducibility of the experiments, the correlation of transcript-level enrichments was evaluated across the three CLIP-seq libraries. The Pearson coefficients between any two of the three libraries were at least 0.93 (Figure S1C), indicating that most of the LIN28A CLIP tags had originated from the common pool of LIN28A-interacting RNAs.

Confirmation of the *Let-7* Family as a Target of LIN28A

Because the *let-7* family miRNAs are the most thoroughly studied targets of LIN28A, they serve as important positive controls for our experiment. As expected, we detected CLIP tags from let-7 precursors in the sequence alignment (Figures 1C and 1D for *Mirlet7g*; see also Figures S2A and S2B for *Mirlet7d* and *Mirlet7f-1*, respectively).

Because it remains unclear whether the *let-7* family is the only miRNA target of LIN28A in mESCs, we analyzed our CLIP-seq library to find other LIN28A-interacting miRNAs. Because there is yet no reliable method to globally quantify the amounts of miRNA precursors, we had to use mature miRNA signals from microarrays for normalization. Despite the technical limitation, the *let-7* family comprises the most enriched group in the CLIP-seq (Figure 1E). Although a few miRNA precursors such as pre-miR-677 and pre-miR-708 showed comparable enrichments, their mature miRNA levels did not change significantly upon *Lin28a* knockdown (Figure 1E and Table S2). Thus, this analysis indicates that, at least in mESCs, the *let-7* family is likely to be the only functional miRNA target of LIN28A.

LIN28A Binds to *Let-7* Precursors through the GGAG Motif

Our previous biochemical study showed that the GGAG motif in the terminal loop of the let-7 precursor serves as the binding center for the CCHC zinc finger domains and is required for specific recognition by LIN28A (Heo et al., 2009). Almost all let-7g CLIP tags contain the GGAG sequence, indicating that our CLIP libraries faithfully reflect physiological interactions between LIN28A and let-7g precursor.

Interestingly, we noticed frequent sequence alterations at the GGAG motif in our CLIP tags (Figures 1C and 1D). Particularly, the first guanosine of the motif is often substituted with other nucleotides. Similar substitution pattern was observed with other let-7 precursors as well (Figures S2A and S2B). Such alteration on a specific site is likely to be an outcome of UV crosslinking to LIN28A because a small piece of crosslinked peptide would remain even after proteinase treatment and interfere with the progression of reverse transcriptase as previously reported (Granneman et al., 2009; Kishore et al., 2011; Zhang and Darnell, 2011).

Crosslinking-Induced Errors Allow Identification of LIN28A Binding Sites at Single-Nucleotide Resolution

Our libraries contain a large number of tags mapped to non-miRNA transcripts, suggesting that LIN28A may interact with other types of RNAs in addition to let-7 precursors. To precisely map the binding sites in such transcripts, we took advantage of the mutations. Substitution and deletion errors are significantly more prevalent in our CLIP-seq libraries (~1.5% for substitution and ~0.5% for deletion) than in the RNA-seq library (~0.25% for substitution and ~0.05% for deletion), whereas insertion errors occur at comparable rates in the two different types of libraries (Figure S2C). Like in the let-7 precursors, most substitutions and deletions in CLIP tags are found on G, whereas error frequencies on A, C, or U are similar to those in RNA-seq library (Figure S2D).

The base substitution in CLIP-seq data is a useful feature that allows mapping of protein binding sites at single-nucleotide resolution. We searched for LIN28A-binding sites on a transcriptome-wide level by using Shannon's information entropy, which quantifies the randomness of nucleotide composition at a given

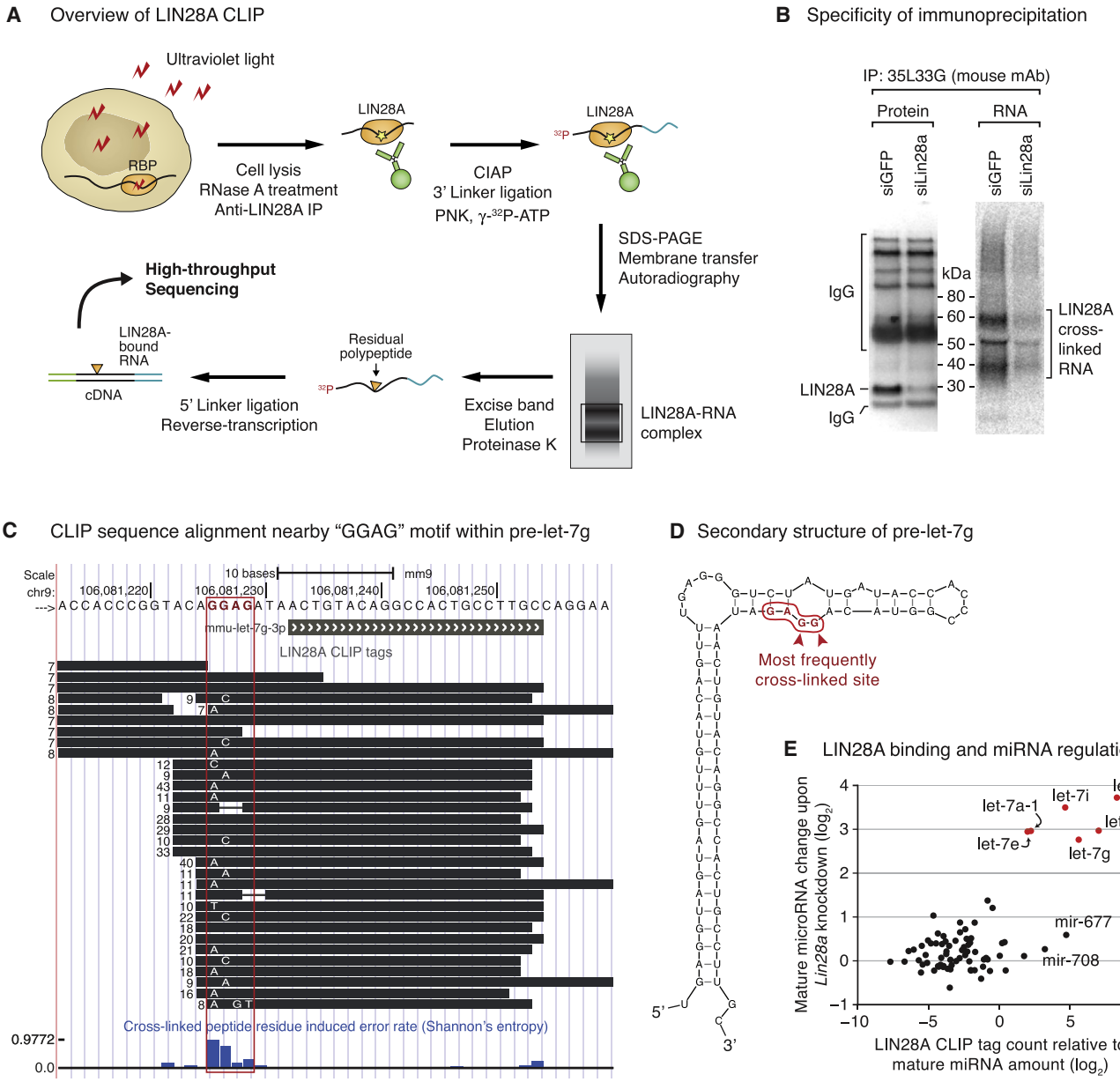

Figure 1. LIN28A CLIP-seq on Mouse Embryonic Stem Cells and Confirmation of the Interaction between LIN28A and let-7 Precursors

(A) LIN28A CLIP-seq workflow. See Extended Experimental Procedures for details. Abbreviations: CIAP, calf intestinal alkaline phosphatase; PNK, polynucleotidyl kinase.

(B) Monoclonal anti-LIN28A antibody, 35L33G, specifically precipitates the LIN28A-RNA complexes. Left: western blot of LIN28A immunoprecipitates from siGFP- or siLin28a-treated A3-1 mESC lysates. Right: autoradiography of 5′-^{32}P-labeled RNAs crosslinked to LIN28A in siGFP- or siLin28a-treated A3-1 cells. Crosslinking-induced mobility shift of LIN28A was not observed in western blotting because only a small fraction of the protein was crosslinked to RNA in CLIP-seq condition.

(C) Sequences from LIN28A CLIP libraries aligned to the let-7g locus. The previously known binding site of LIN28A, the GGAG motif in the terminal loop of precursor let-7g, is marked with a red box. Each unique sequence is represented by a black horizontal bar with the number of reads indicated on the left. Mismatched sequences are shown in white letters. Site mutation rate is quantified by using Shannon's entropy and is shown at the bottom with blue bars. Less frequent tags (<7 reads) are omitted to improve visibility. See Figures S2A and S2B for other *let-7* loci.

(D) Predicted secondary structure of pre-let-7g with the GGAG motif shown in red. The red arrowheads indicate the binding sites of LIN28A detected in our CLIP experiments.

(E) A scatter plot of LIN28A CLIP-seq enrichment levels (x axis) and miRNA level changes after *Lin28a* knockdown (y axis). The CLIP tag counts for miRNA loci were normalized by using the sum of miRNA microarray signals from the 5′- and 3′-arms. See also Figures S1 and S2 and Table S1.

A LIN28A binding motif

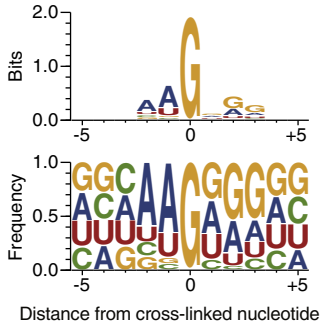

B Top 10 LIN28A-interacting hexamers

Sequence	Frequency (%)
AAGGAG	8.03
AAGGUG	3.91
AAGAGG	3.76
AAGAAG	3.61
AAGAGA	2.49
AAGAGC	2.11
AAGCAG	2.00
AAGUGG	1.69
AAGAGU	1.53
GAGGAG	1.44

D Top 10 sequences flanking hexamers

Sequences	Frequency (%)
CC.....GG	3.50
GG.....CC	2.84
GC.....GC	2.81
AG.....CU	2.52
UC.....GA	2.14
CA.....UG	1.95
GA.....UC	1.41
CU.....AG	1.41
AC.....GU	1.41
GG.....CU	1.32

C Similarity network of LIN28A-bound enriched hexamers

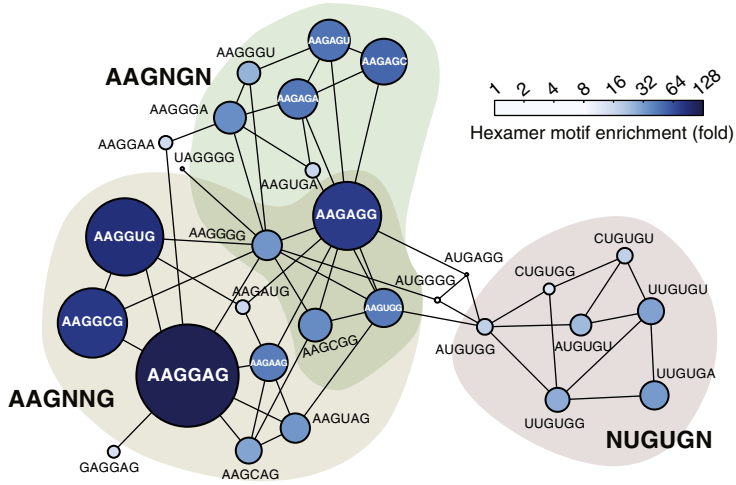

E Normalized relative frequency of Watson-Crick pair between two bases flanking LIN28A binding sites

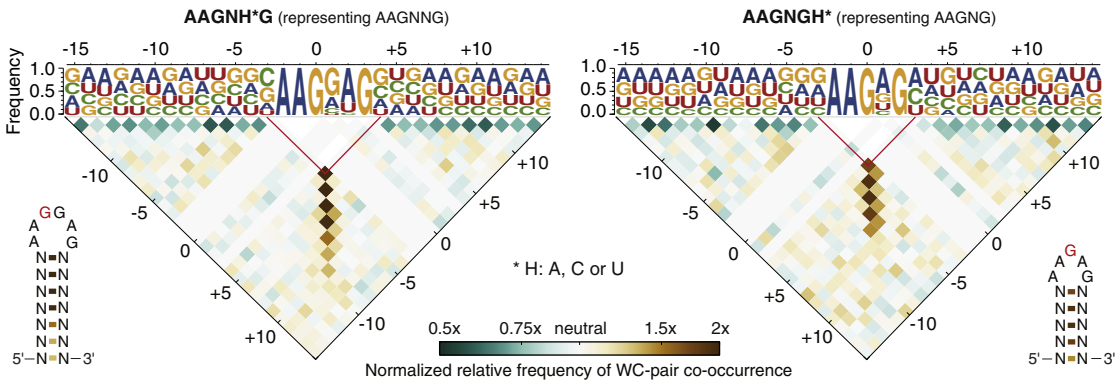

Figure 2. Identification of LIN28A Binding Motifs

(A) LIN28A binding motif identified by CLIP-seq. Sequences harboring a mutation were aligned with the mutated nucleotide centered at zero. The information content (top) and positional frequency (bottom) are visualized by using WebLogo (Crooks et al., 2004). See also Figure S3C for a wider view and individual biological replicates.

(B) List of ten most frequently observed LIN28A-interacting hexamers from the CLIP-seq.

(C) Clusters of LIN28A-interacting hexamers. Area and color of each node represent relative enrichment of the hexameric sequence compared to the background frequency from RefSeq transcripts. Any two connected nodes differ by a single nucleotide. With few exceptions, hexamers can be grouped into three clusters: AAGNNG, AAGNG(N), and (N)UGUG(N) where N = A, C, G, or U.

(D) List of ten most frequently observed 2 nt sequence pairs flanking LIN28A-bound hexamers. Note that the flanking sequences can base pair with the nucleotides at the opposite side of the hexamer.

position. It reduces false positives derived from single-nucleotide polymorphism or paralogous genes, which generally cause only one or two types of substitutions rather than all three possible substitutions (i.e., G to A, C, or T). The mutation rate quantified by Shannon's entropy correlates with the enrichment level of the given site in CLIP-seq, albeit modestly (Figure S3A), which further supports our notion that the mutated sites are derived from genuine LIN28A binding sites.

Altogether, we identified 516,259 putative binding sites with the confidence level of 0.1% false discovery rate (FDR) (Figure S3B and Table S3A), which means that a confident LIN28A binding site occurs at every 21.7 guanosines. On average, 38.5 sites were detected per mRNA. This unexpectedly large number of binding sites suggests that LIN28A binding is not restricted to a few sites on a small group of RNAs. Rather, LIN28A interacts with a large proportion of transcriptome.

LIN28A Favors Single-Stranded Purine-Rich Motifs

To better understand LIN28A-RNA interactions, we further analyzed patterns around the potential LIN28A binding sites (Figures 2A and S3C). The frequently mutated G is preceded by two bases with strong preference for A or U and is followed by three bases favoring G or A. We also observed clear depletion of C across the hexamer. The resulting consensus sequence in the WebLogo is "AAGNGG" (Figure 2A). Unexpectedly, this consensus is different from the most frequently observed hexamer, "AAGGAG" (Figure 2B and Table S3B). We reasoned that the consensus may actually be a mixture of multiple distinct motifs. Indeed, similarity network of the LIN28A-bound hexamers revealed three distinct clusters, AAGNNG, AAGNG(N), and (N)UGUG(N) (Figure 2C). The "AAGNNG"-type hexamers account for the majority of LIN28A binding sites. This is consistent with the recent structural study that showed that the two zinc finger motifs of LIN28A recognizes "AGNNG" (Loughlin et al., 2012). The "AAGNG"-type pentamers also appear, albeit with lower frequency. Note that the least prevalent "UGUG" motif has not been reported before and may reflect a different mode of LIN28A binding. We further validated these three motifs by carrying out electrophoretic mobility shift assay (EMSA) with recombinant LIN28A protein and chemically synthesized RNA segments (Figure S4). Three representative RNAs containing the AAGGAG, AAGAG, and UGUG elements interacted with LIN28A, with UGUG being the weakest binder. Mutations to the G residue (that is frequently substituted in CLIP-seq) strongly reduced the affinity toward LIN28A, confirming that the identified motifs provide genuine binding sites for LIN28A.

Because, in the case of pre-let-7, the GGAG motif is invariably located in the terminal loop near the stem (Heo et al., 2009), and our EMSA data show that the stem of pre-let-7 enhances the binding of LIN28A (Figure S4); we examined the secondary structure around the binding motif. Interestingly, the sequences upstream of the hexamers are often complementary to the other side of the hexamer (Figure 2D). The bases surrounding AAG NNG-type binding sites have clear propensity to form Watson-Crick (WC) pairs compared to randomly permuted sequences (Figure 2E, left). Moderate but significant enrichment was observed between bases that are up to seven nucleotides from the LIN28A-interacting hexamers, indicating that the stem surrounding the hexamer is around 7 bp in length. Similarly, the AAGNG pentamer is located in the terminal loop of a stem-loop structure with a slightly shorter stem (~5 bp) (Figure 2E, right). It is noted that some binding sites are in single-stranded RNA regions of more complex structures such as branched hairpins.

The preference of LIN28A for a hairpin structure is further supported by folding energy analysis (Figure S3D). Stronger structures (lower free energy) tend to appear more frequently in the CLIP libraries than those with weak structure (Figure S3D). The hairpin structure may help present the LIN28A-recognition element in a more accessible manner. Together, our analyses indicate that LIN28A preferably binds to a "AAG(N)NG" motif located in the terminal loop of a hairpin with a stem of 5–7 bp.

When we looked at all AAGGAG instances within a stem-loop structure in abundantly expressed mRNAs, almost half of the instances (41.7% with a cutoff of free energy of −6 kcal/mol) were experimentally detected in our CLIP-seq (Figure S3E). Other frequently observed motifs were also detected at similar rates when combined with low free energy cutoff (Figure S3E). This suggests that the motifs identified from our analyses may indeed be sufficient for LIN28A binding as long as the binding site is accessible to LIN28A in the cell.

Messenger RNAs Are the Major LIN28A Targets

Next, we analyzed the types of RNAs that interact with LIN28A. Among the RNAs in the LIN28A CLIP-seq libraries, mRNAs constituted the most enriched class—over 42% of the tags were mapped to mRNAs, whereas miRNA loci made up only 0.07% of the sequenced reads (0.05% came from *let-7* loci) (Figure 3A and Table S4). The second most abundant class was ribosomal RNA, which occupied 17% of the CLIP tags. However, considering the overwhelming amount of rRNAs in cells (~80% of total RNA), our result indicates that mRNAs are the major interactors of LIN28A.

Within mRNAs, intronic regions are strongly depleted in CLIP tags (Figure 3B), indicating that LIN28A interacts with mature mRNAs after splicing is completed. We also analyzed the average density of the CLIP tags around start and stop codons (Figure 3C). The metagene analysis showed significant depletion of LIN28A binding in the 5′ UTR compared to the coding sequences (CDS) and the 3′ UTR.

LIN28A Reduces Ribosome Occupancy without Affecting mRNA Abundance

To understand the functional significance of mRNA-LIN28A interaction, we first considered a possibility that LIN28A may

(E) Normalized relative frequency matrix of WC-pair co-occurrence around LIN28A-interacting sequences. Left and right panels represent the matrix for AAGNNG and AAGNG motifs, respectively. The actual motif patterns were reduced to AAGNHG and AAGNGH (where H = A, C, or U) to avoid interference between the two motifs. Sequences are aligned such that the crosslinked bases are centered at zero. Nucleotide frequency is presented above the triangular matrix. Colors in the triangular matrix, indicating WC-pair enrichment or depletion, are normalized to the background frequency estimated by permutation. See also Figures S3 and S4 and Tables S2 and S3.

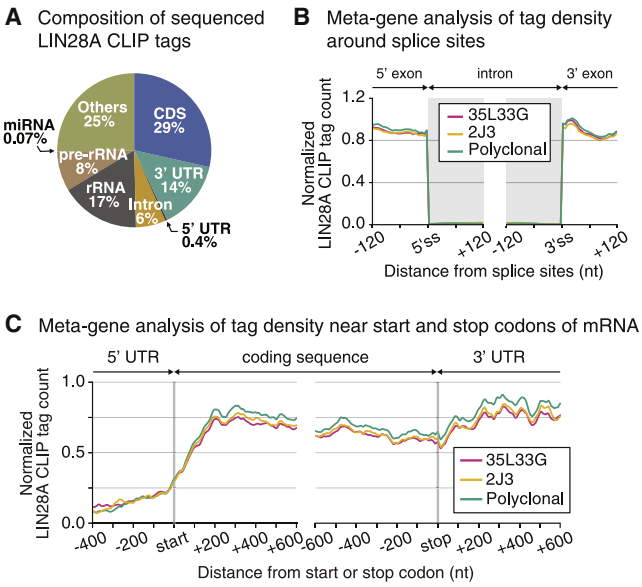

Figure 3. Messenger RNA as a Major Class of LIN28A Targets

(A) Classification of LIN28A CLIP tags from the 35L33G (mAb) experiment. See also Table S4 for full description of classified annotations.

(B) CLIP tag density near splice sites (ss). The density was normalized per ss by mean alignment depth of exonic regions in the window (120 nucleotides from each of 5′ ss and 3′ ss) in RNA-seq.

(C) Density of LIN28A CLIP tags across different regions of mRNAs. Tag counts were normalized by RPKM in RNA-seq.

regulate the abundance of its targets. However, when we measured mRNA levels by RNA-seq after *Lin28a* knockdown, we could not find a significant correlation between CLIP tag enrichment (representing LIN28A binding; Figure 4A, x axis) and the changes in mRNA levels (Figure 4A, y axis). Therefore, LIN28A is unlikely to be involved in the stability control of its target mRNAs.

We next asked whether LIN28A regulates translation. LIN28A has previously been shown to be associated with polysomes in mouse teratocarcinoma P19 (Balzer and Moss, 2007) and in the differentiating mouse myoblast cell line, C2C12 (Polesskaya et al., 2007). Also, LIN28A is known to be a positive regulator of translation for mRNAs such as *Igf2*, cyclin A, cyclin B, histone 2a, and *Oct4* (Polesskaya et al., 2007; Qiu et al., 2010; Xu and Huang, 2009; Xu et al., 2009). Consistent with the previous observations, we found that LIN28A comigrates with polysome in mESCs (Figure 4B).

In order to monitor translational efficiency at the genomic level, we performed ribosome footprinting after *Lin28a* knockdown (Guo et al., 2010; Ingolia et al., 2009). Briefly, mESCs were transfected with control siRNA (siLuc) or siLin28a and were incubated for 48 hr prior to cycloheximide treatment and cell lysis (Figure 4C). The cell lysates were treated with RNase I to remove mRNAs that are not protected by ribosomes. The protected part of mRNA (the "footprints" of ribosomes) were retrieved by linker ligation and deep sequencing. Our experiment was successful judging from the characteristic enrichment of ribosome footprints in CDS (Figure S5A) and the three-nucleotide periodicity (Figure S5B).

Interestingly, there is a strong positive correlation between LIN28A interaction (Figure 4D, x axis) and ribosome density change (Figure 4D, y axis) ($p = 1.01 \times 10^{-188}$, Pearson's correlation test). That is, ribosome occupancy of LIN28A-bound mRNAs tends to be higher in *Lin28a*-depleted cells compared to that in control siRNA-treated cells (Figures 4D, 4E, and S5C). This result indicates that LIN28A may negatively regulate the translation of its target mRNAs. This is surprising given that LIN28A is known as a positive regulator of translation (Polesskaya et al., 2007; Qiu et al., 2010; Xu and Huang, 2009; Xu et al., 2009). To validate the result, we carried out western blotting for genes whose ribosomal density increased or decreased after *Lin28a* knockdown without a change in the mRNA levels (Figure S5D and Table S5). The mRNAs coding LAMP1, EpCAM, and E-cadherin interact with LIN28A, whereas the other three mRNAs are not significantly enriched in CLIP. The changes in protein levels (monitored by western blotting, Figure S5D) are consistent with the ribosomal density changes (determined by ribosome footprinting, Table S5), indicating that LIN28A indeed targets mRNAs for translational repression.

Of note, under our experimental conditions (knockdown for 48 hr), let-7 targets were not significantly affected in either mRNA abundance or ribosome occupancy (Figure S5E). Thus, LIN28A may act directly on translation of its target mRNAs independently of its effect through let-7.

LIN28A Targets mRNAs Destined for Endoplasmic Reticulum

We next performed gene ontology (GO) analysis to understand functional consequences of LIN28A-mediated translational control (Figure 5A). This analysis revealed strong enrichment of several terms, with most biased GO terms related to cellular components. Interestingly, the majority of LIN28A targets are integral membrane proteins, secretory proteins, and ER or Golgi apparatus localized proteins (Figure 5A and Tables S5 and S6). These proteins are commonly translated in the ER-bound ribosomes and translocated into ER cotranslationally. In contrast, genes associated with nucleus and cytoplasm that are translated by free cytosolic ribosomes are underrepresented in the CLIP libraries (Figure 5A, x axis), and their translation is unaffected in LIN28A-depleted cells (Figure 5A, y axis). Considering the normalization issue caused by a shift of other groups, the modest changes associated with nuclear and cytoplasmic proteins are unlikely to be significant. Of note, CLIP enrichment of nucleosomal proteins is overestimated because histone mRNAs are depleted in RNA-seq data due to the lack of poly(A) tail. Taken together, LIN28A may preferentially bind to and control the mRNAs that are translated on ER.

Translation of most ER-associated mRNAs begins in the cytosol but halts once the signal sequence is synthesized. Signal-recognition particle (SRP) binds to the signal sequence and guides the mRNA-ribosome complex to the surface of ER where translation resumes and the nascent polypeptide is simultaneously translocated into the ER (Deshaies et al., 1991). We found that mRNAs encoding integral membrane proteins, which comprise the majority of the ER-associated translation, interact with LIN28A about four- to six-fold more frequently than other mRNAs do (Figures 5B and S6A, x axes; $p = 3.08 \times 10^{-33}$,

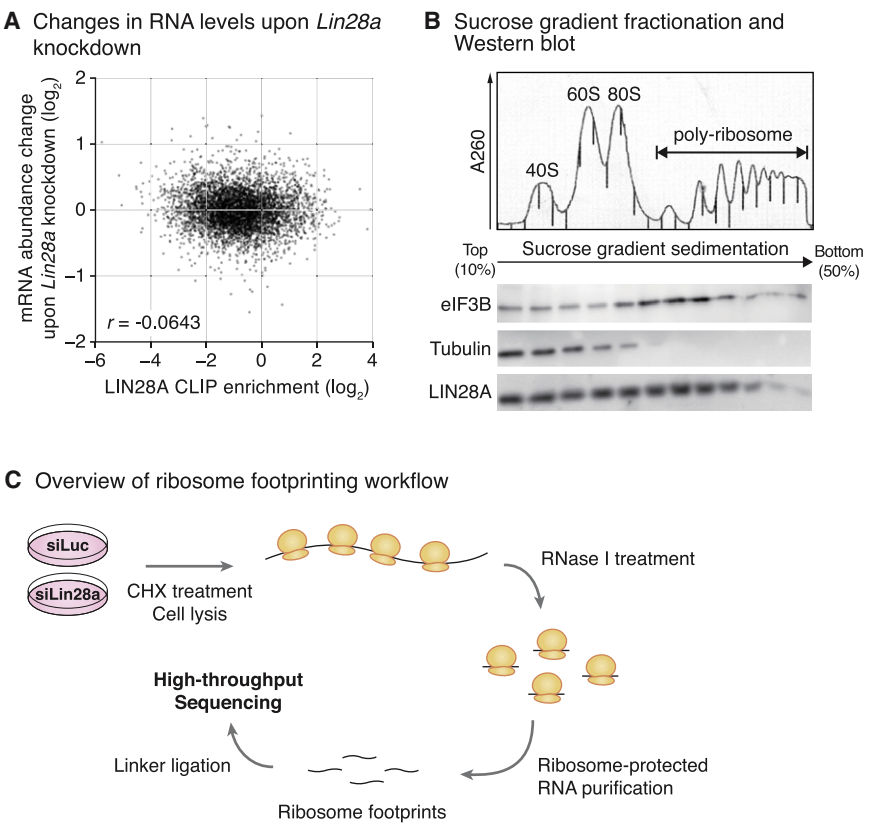

Figure 4. Ribosome Occupancy Is Controlled by LIN28A-Binding

(A) A scatter plot showing the correlation between CLIP tag enrichment and RPKM change upon *Lin28a* knockdown. Each point represents a single RefSeq transcript.

(B) Sucrose gradient fractionation of A3-1 mESC lysates. Absorbance at 260 nm was recorded while each fraction was collected. The locations of 40S subunit, 60S subunit, monosome, and poly-ribosome were determined by the characteristic pattern of UV absorbance. The protein levels of eIF3b, tubulin, and LIN28A in each fraction were determined by western blotting.

(C) Workflow of ribosome footprinting. CHX is an abbreviation for cycloheximide.

(D) A scatter plot showing the correlation between CLIP enrichment and the change of ribosome footprint density in LIN28A-depleted cells.

(E) Cumulative distributions of ribosome density changes (alternative representation of D). The patterns for strong binders are clearly different from those with lower CLIP tag enrichment ($p = 2.04 \times 10^{-10}$ between top 5% and 20%–50% interval and $p < 10^{-320}$ between top 5% and bottom 50%, Kolmogorov-Smirnov test). See Figure S5C for the results derived from different LIN28A antibodies. See also Table S4.

Mann-Whitney U test). Furthermore, their translation becomes more active compared to the other genes when *Lin28a* is knocked down, indicating that they are the major functional targets of LIN28A in translational control (Figures 5B and S6A, y axes; $p = 6.97 \times 10^{-106}$, Mann-Whitney U test). To validate the result, we carried out metabolic labeling after *Lin28a* knockdown and measured ^{35}S-methionine incorporation in rough ER (RER) microsome fraction (Hamilton et al., 1999) (Figure 5C). In LIN28A-depleted cells, protein synthesis rate was increased in RER fraction that is enriched with membrane proteins, indicating that LIN28A may indeed suppress ER-associated translation.

It is noted that mRNAs encoding tail-anchored transmembrane proteins behave differently from other ER-associated mRNAs. Unlike typical membrane proteins, these proteins are synthesized in the cytosol and translocated to ER posttranslationally (Kutay et al., 1993). Our data show that tail-anchored transmembrane proteins are neither enriched in LIN28A CLIP-seq nor increased in ribosome density in LIN28A-depleted cells (Figures 5D and S6B). This pattern is similar to other mRNAs that are translated by free cytosolic ribosomes. Thus, this result reinforces our conclusion that LIN28A differentially acts on ER-associated translation.

To understand the selectivity of the regulation, we asked whether ER-associated mRNAs carry more LIN28A-recognition motifs than non-ER-associated mRNAs do. For this analysis, we first predicted the LIN28A-recognition sites on all mRNAs by using a hidden Markov model. To train the model, we used the binding sites experimentally identified from our CLIP-seq (see Figure S3F and Table S7 for the result and Extended Experimental Procedures for detail). Surprisingly, when we applied the model to predict potential LIN28A-interacting sites, non-ER-associated mRNAs harbor as many predicted sites as ER-associated mRNAs do (Figure S6C), indicating that the sequence and the structural features of ER-associated mRNAs are indistinguishable from those of non-ER-associated mRNAs. Nonetheless,

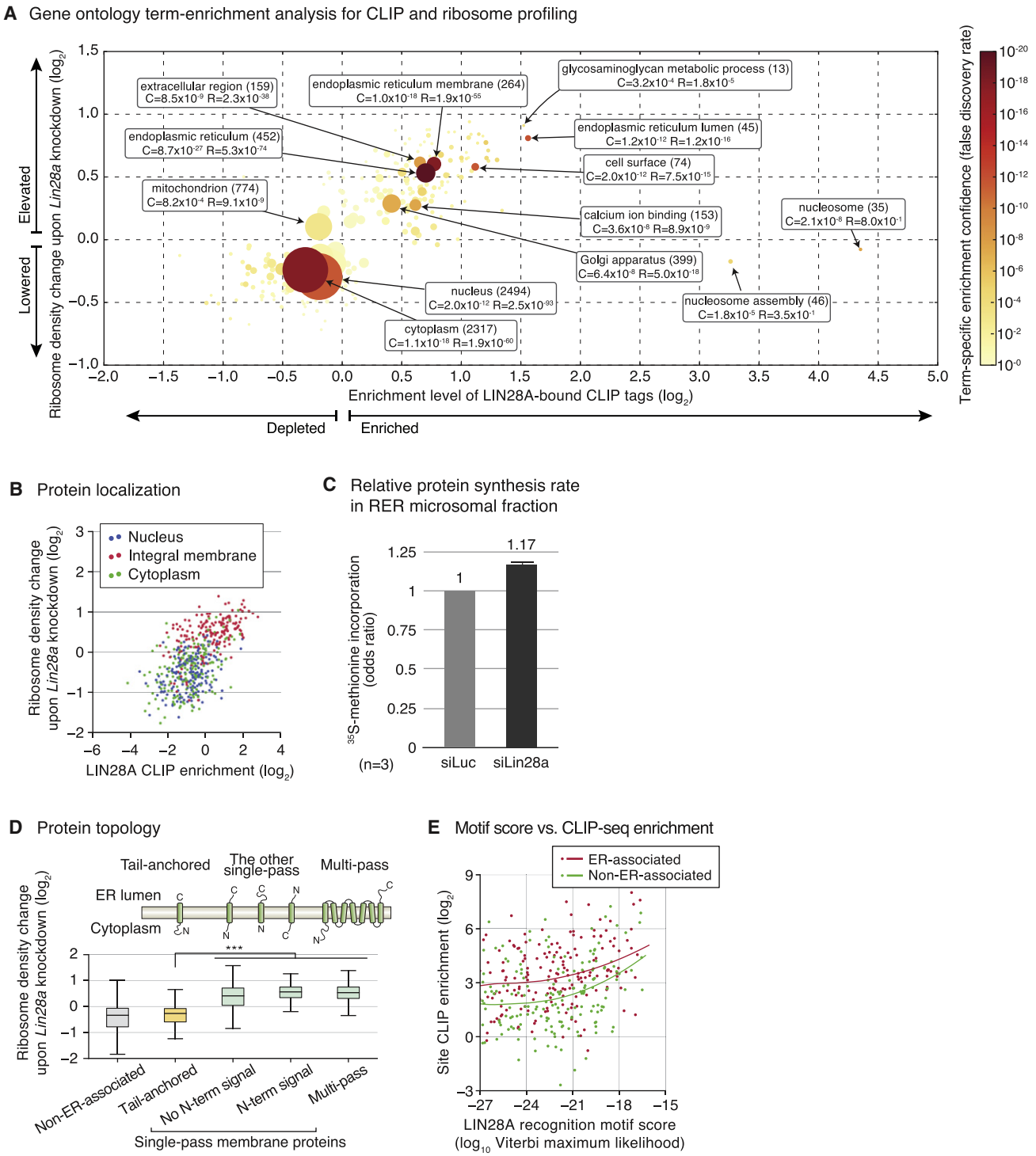

Figure 5. LIN28A CLIP-seq and Ribosome Footprinting Suggests ER-Associated Translation

(A) GO enrichment analysis for CLIP-seq and ribosome footprinting data. Each circle represents a GO term. The color intensity indicates statistical significance of enrichment or depletion determined by Mann-Whitney U test. The size of the circle corresponds to the number of genes, whereas the coordinates indicate average CLIP tag enrichment (x axis) and ribosome density change (y axis). Balloons contain the number of genes (written in parentheses) and p values for CLIP-seq (C) and ribosome footprinting (R). Note that nucleosome-related terms are overestimated artificially in CLIP because of a normalization problem due to the lack of polyA tail in histone mRNAs.

(B) Specificity of LIN28A targeting. mRNAs encoding integral membrane proteins are enriched in CLIP libraries (x axis) and affected most significantly in ribosome density upon *Lin28a* knockdown (y axis). This plot shows 200 randomly chosen transcripts per term for better visibility, and the original plot is available in Figure S6A.

when we compared the sites with comparable motif scores, the sites on ER-associated mRNAs are detected by CLIP-seq more frequently than those on non-ER-associated mRNAs (Figures 5E and S6D; $p = 3.46 \times 10^{-85}$, two-way ANOVA). These results indicate that LIN28A-recognition element itself may not be sufficient to explain the preference for ER-associated mRNAs. In other words, there should be additional factor(s) that influences the interaction between LIN28A and its targets.

LIN28A Is Localized in Peri-ER Area

We postulated that the preference for ER-associated mRNAs might be, at least in part, due to nonuniform subcellular distribution of LIN28A. Indeed, immunocytochemistry revealed that LIN28A is localized in the peri-ER area in mESCs. LIN28A signal is detected in the region surrounding ER that is marked by proteins containing ER-retention signal (KDEL) (Figure 6A, upper). Distribution of LIN28A is distinct from that of a cytosolic protein, GAPDH, which is more widely spread in the cytosol (Figure 6A, lower). For better visualization of the cytoplasmic compartment, we also examined ectopically expressed LIN28A in HeLa cells whose cytoplasm is larger than that of mESCs. Like the endogenous protein in mESCs, ectopically expressed LIN28A is enriched near ER in HeLa cells (Figure 6B).

We also carried out subcellular fractionation and found that LIN28A is present in the microsomal fraction derived from rough ER (RER) (Figure 6C) (Hamilton et al., 1999). Although cytosolic proteins such as tubulin and the cleaved fragment of ATF6 are not detected in the RER microsomal fraction, a significant amount of LIN28A is present. Calnexin and the uncleaved form of ATF6 were used as controls for ER membrane proteins. These results indicate that LIN28A may be bound to the cytosolic surface of RER on which ER-associated mRNAs are translated. Due to the colocalization, LIN28A may interact with ER-associated mRNAs more frequently than with other mRNAs.

DISCUSSION

CLIP-seq technology allowed us to map the LIN28A binding sites on the genomic scale at single-nucleotide resolution. A recent study used a combination of coimmunoprecipitation (without crosslinking), oligo-dT enrichment, and deep sequencing, in order to find LIN28A targets in human ESCs (Peng et al., 2011). When we compared the published data with our results, we did not find significant overlap between the two data sets (Figure S7A). It is currently unclear why the data sets are so different. But given that the simple coimmunoprecipitation method is vulnerable to indirect interaction (Ule et al., 2005) and nonphysiological binding of RNAs (Mili and Steitz, 2004) and that genuine targets may be lost depending on washing conditions unless they are crosslinked to protein (Licatalosi and Darnell, 2010; Ule et al., 2005), our data may provide a more accurate list of LIN28A targets. In support of the notion, the LIN28A binding motif found in our CLIP-seq analysis is highly similar to that found in previous biochemical and structural studies on let-7 precursors. Moreover, we provide additional genome-wide functional evidence using ribosome footprinting, which demonstrates that the mRNAs identified in our study are indeed functional targets of LIN28A.

One of the key advantages of using the CLIP-seq approach is that one can map the binding sites by taking advantage of mutated sequences. Our study reveals the LIN28A-binding elements: AAGNNG (with the most frequent sequence being AAG GAG) placed in the terminal loop of a small hairpin structure. According to the structural studies (Loughlin et al., 2012; Nam et al., 2011), the first G (that is most frequently mutated) forms a hydrogen bond with Lys160 in the zinc finger motif, which may be the actual crosslinking residue in our CLIP experiment. Another RNA binding domain, cold-shock domain (CSD), that is in the N-terminal part of LIN28A was reported to interact with a GNGAY motif located in the upstream of the GGAG motif of pre-let-7 (Nam et al., 2011). However, we did not find a significant enrichment of any motif upstream of the AAGNNG element (data not shown). The CSD-RNA interaction may not have been captured by CLIP-seq partly because CSD interacts with RNA with very low sequence specificity (Heo et al., 2009; Nam et al., 2011). Due to the low complexity of the recognition element and the high abundance of LIN28A protein in ESCs, it is not surprising that we identify so many LIN28A binding sites in our CLIP-seq experiment (38.5 sites per mRNA). Our study suggests that LIN28A may bind to many mRNAs and dampen their usage rather than acting as an on-off switch for a small set of RNAs.

Our analyses indicate that the aforementioned motif may not be sufficient to predict which RNA is targeted by LIN28A because the actual interaction inside the cell is strongly influenced by the local concentration of the interactants (Figure 7A). Because of the localization of LIN28A in the peri-ER area, LIN28A may encounter ER-associated mRNAs more frequently than those distributed throughout the cytosol. Therefore, the selectivity at the transcript level may be dictated mainly by the intracellular localization of the transcript. The LIN28A-recognition element, on the other hand, determines which mRNA among the local pool interacts with LIN28A more frequently than other RNAs and which position on the given transcript LIN28A is loaded onto. Not mutually exclusively, peri-ER localization of LIN28A may be reinforced by its interaction with mRNAs

(C) Protein synthesis rate was measured by ^{35}S-methionine incorporation in the fraction enriched with RER microsome (RER) and normalized against that in the remaining lysate. The result suggests that membrane protein synthesis was increased upon knockdown of *Lin28a* ($n = 3$; $p = 0.0032$, one-tailed paired t test). The error bar represents SD of the normalized ratios from biological triplicates.

(D) Box plot of ribosome density changes of genes that are grouped according to protein topology. Tail-anchored membrane proteins remain unaffected, whereas other transmembrane proteins increase in ribosome density ($p = 3.76 \times 10^{-23}$, Mann-Whitney U test). Transmembrane proteins targeted to organelles other than ER were excluded from this analysis.

(E) Scatter plot of motif score of the binding sites (predicted by HMM using sequence and structure information) and their enrichment level in CLIP-seq relative to RNA-seq. Red dots represent CLIP-identified LIN28A binding sites on ER-associated mRNAs, whereas green dots represent those on non-ER mRNAs. To improve visibility, 200 sites with relatively high scores ($\log_{10}$ maximum likelihood > -27) were randomly chosen from each group. The complete representation is available in Figure S6D. See also Tables S5, S6 and S7.

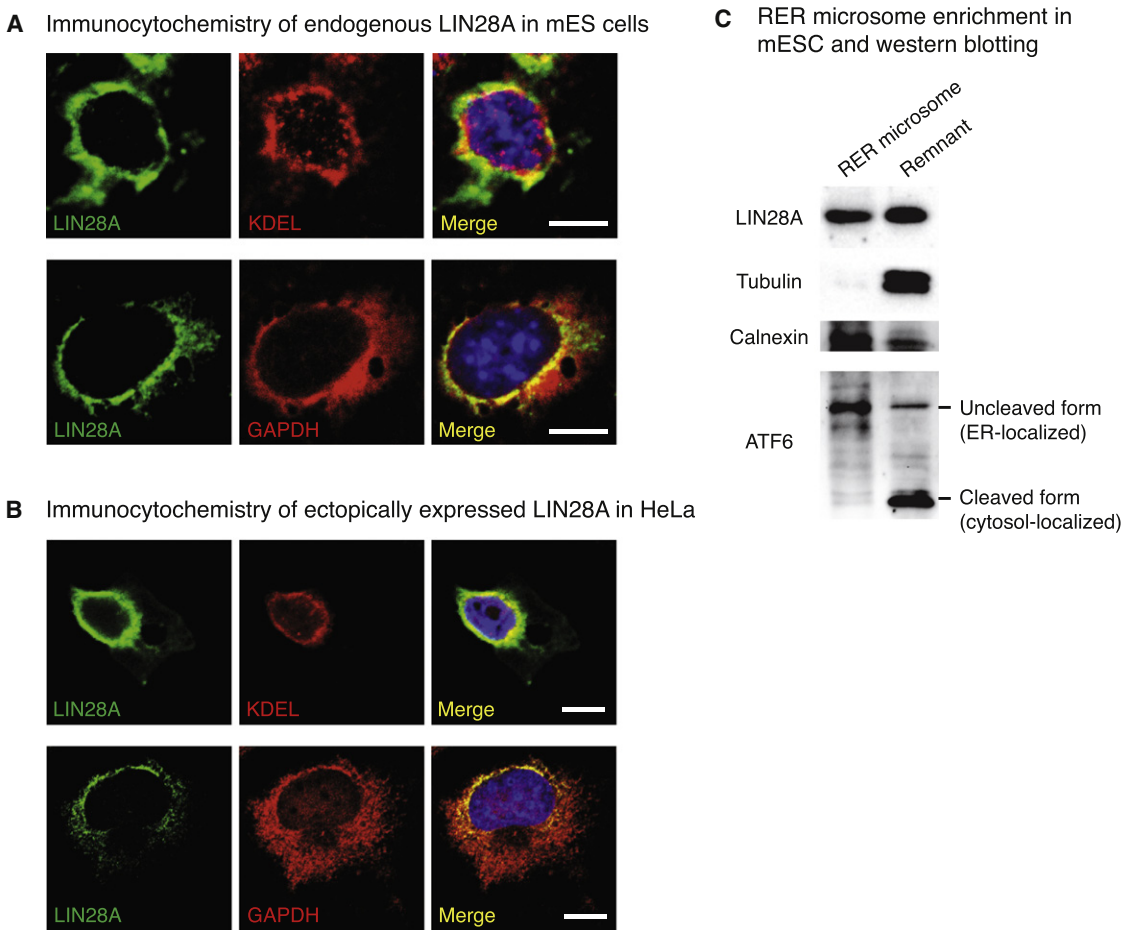

Figure 6. LIN28A Is Enriched in Peri-ER Area

(A) Immunofluorescence of endogenous LIN28A and ER marker (KDEL peptide) in A3-1 mESCs. GAPDH was used as a control to show the distribution of a cytosolic protein. Scale bar, 10 μm.

(B) Immunofluorescence of ectopically expressed LIN28A and endogenous ER marker (KDEL peptide) in HeLa. GAPDH was used as a control to show the distribution of a cytosolic protein. Scale bar, 10 μm.

(C) Western blot analysis of the fraction enriched with microsomes derived from RER in A3-1 mESCs. The remaining fraction (remnant) was loaded as a control. Calnexin and uncleaved ATF6 are used as ER markers, whereas tubulin and cleaved ATF6 are representatives of free cytosolic proteins. LIN28A is significantly enriched in rough ER microsomal fraction compared to other cytosolic proteins.

concentrated near ER area. It remains to be investigated how LIN28A is transported and maintained in the peri-ER region. It will be interesting to identify and study the functions of the proteins that interact with LIN28A.

Ribosome footprinting provides evidence that LIN28A acts mainly as a suppressor rather than an enhancer of translation. Although we observe some genes that may be positively controlled by LIN28A, they constitute a minor fraction among LIN28A binders. It will be of interest to learn the mechanism by which LIN28A interaction leads to translational inhibition. Because interacting sites typically occur throughout coding sequences and 3′ UTR at multiple locations, LIN28A may interfere with a step prior to or during elongation. To our knowledge, LIN28A is the first example of an mRNA-binding protein that represses ER-associated translation. Further investigation of the action mechanism of LIN28A may offer new insights into the control of ER-associated translation and help us to uncover the regulatory machineries.

Our study reveals an unexpected role of a stem cell factor in the ER secretory pathway (Figure 7A). A recent report from the Weissman lab showed that translational efficiency of integral membrane proteins is significantly lower in undifferentiated ESCs compared to differentiating embryoid bodies (EBs) (Ingolia et al., 2011). Because *Lin28a* is downregulated in EBs, the data collectively suggest that LIN28A may be responsible at least partially for the global translational suppression of membrane proteins in ESCs. When we compared our results with the data from ESCs and EBs (Ingolia et al., 2011), we found significant overlap between the two data sets (Figures 7B, S7B and S7C). The genes that are translationally upregulated during EB differentiation tend to be enhanced translationally in LIN28A-depleted ESCs. The correlation was significant, especially for mRNAs that

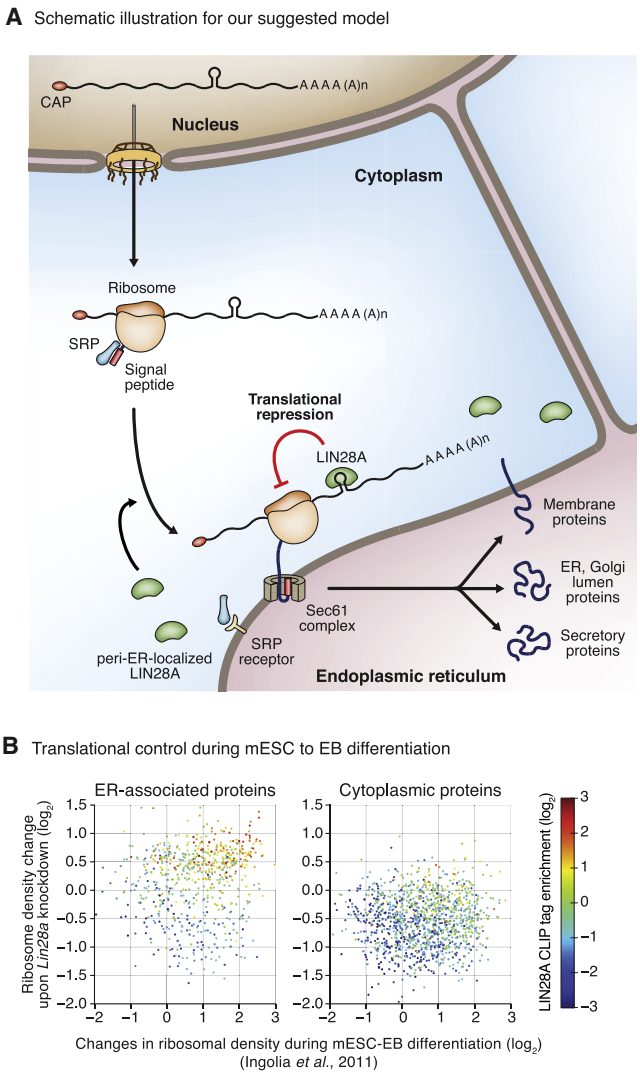

Figure 7. Translational Suppression by LIN28A in Embryonic Stem Cells

(A) Model for the regulation of ER-associated translation by LIN28A. ER-associated mRNAs are transported to ER via SRP pathway. Because LIN28A is localized in peri-ER region and it preferentially binds to the ER-associated mRNAs. The binding also depends on whether the mRNA contains a motif (AAGNNG on a small hairpin) that is optimal for LIN28A binding.

(B) Comparison between the changes in ribosome density upon *Lin28a* knockdown (y axis, our data) and those during mESC-EB differentiation (x axis; Ingolia et al., 2011). Each dot represents ribosome density change (position) and LIN28A CLIP enrichment level (color). Strong LIN28A binders (red dots) tend to be derepressed significantly in both conditions. See also Figure S7B for proteins targeted to nucleus and mitochondria.

were strongly bound to LIN28A (based on CLIP-seq data) (Figure 7B, red dots). The CLIP enrichment score correlates with translational changes accompanying the ES-EB differentiation ($p = 6.85 \times 10^{-202}$, Spearman's rank correlation test). Because none of the common pluripotency markers was decreased under our conditions (48 hr after transfection) (Figure S7D), the observed effects on translation in our experiments are likely to be a consequence of LIN28A depletion rather than an indirect effect of differentiation.

Our data suggest that LIN28A may contribute to the global translational suppression of ER-associated mRNAs in undifferentiated stem cells. This type of regulation may reduce cell surface receptors and secretory proteins, which may influence cell signaling. One may also envision that global suppression of ER may be a way of redirecting cellular resources (such as energy and amino acids) to promote cell autonomous functions such as cell proliferation. It is currently unclear whether and how such regulation contributes to pluripotency and malignancy, but it will certainly be an intriguing arena to investigate.

EXPERIMENTAL PROCEDURES

CLIP-seq

LIN28A CLIP-seq was performed by using mouse embryonic stem cell A3-1 (Suzuki et al., 1997) as described in Extended Experimental Procedures. Two mouse monoclonal antibodies raised in-house (35L33G and 2J3) and one rabbit polyclonal antibody (Abcam, 46020) were used to construct three biological replicates of CLIP-seq libraries.

Ribosome Footprinting

Ribosome footprinting libraries were generated from siLuc- or siLin28a-transfected A3-1 cells as described previously (Guo et al., 2010). Detailed process is described in Extended Experimental Procedures.

RNA-seq

RNA-seq was performed with the RNA from untreated, siLuc, or siLin28a transfected A3-1 cells. mRNAs were poly-A enriched, fragmented to 35–55 bp, and sequenced.

Sequence Analysis

The cDNA libraries described above were sequenced with Illumina Genome Analyzer II or IIx. Sequence reads were aligned to mouse genome (*mm9* assembly) and RefSeq transcripts by using GSNAP version 2012-01-11 (Wu and Nacu, 2010). Subsequent analyses were performed with in-house software as described in Extended Experimental Procedures. Complete source code and scripts written for this paper are available for downloading at https://github.com/hyeshik/nrclip under MIT-style license.

ACCESSION NUMBERS

The NCBI Gene Expression Omnibus (GEO) accession number for the microarray and high-throughput sequencing data reported in this paper is accession number GSE37114.

SUPPLEMENTAL INFORMATION

Supplemental Information includes Extended Experimental Procedures, seven figures, and seven tables and can be found with this article online at http://dx.doi.org/10.1016/j.cell.2012.10.019.

ACKNOWLEDGMENTS

We are grateful to Huili Guo for advice on ribosome profiling and Daehyun Baek for critical comments on the manuscript. We also thank Ahyoung Cho and Yun Cheng Chang for technical help and members of our laboratory for discussion. This work was supported by the Research Center Program (EM1202) of IBS (Institute for Basic Science); the BK21 Research Fellowships (J.C., H.C., S.C.K., and B.K.) from the Ministry of Education, Science and Technology of Korea; the TJ Park Postdoctoral Fellowship (Y.K.); and the National Honor Scientist Program (20100020415) through the National Research Foundation of Korea (NRF).

Received: July 17, 2012
Revised: September 8, 2012
Accepted: October 1, 2012
Published online: October 25, 2012

REFERENCES

Balzer, E., and Moss, E.G. (2007). Localization of the developmental timing regulator Lin28 to mRNP complexes, P-bodies and stress granules. RNA Biol. *4*, 16–25.

Balzer, E., Heine, C., Jiang, Q., Lee, V.M., and Moss, E.G. (2010). LIN28 alters cell fate succession and acts independently of the let-7 microRNA during neurogliogenesis in vitro. Development *137*, 891–900.

Chi, S.W., Zang, J.B., Mele, A., and Darnell, R.B. (2009). Argonaute HITS-CLIP decodes microRNA-mRNA interaction maps. Nature *460*, 479–486.

Crooks, G.E., Hon, G., Chandonia, J.M., and Brenner, S.E. (2004). WebLogo: a sequence logo generator. Genome Res. *14*, 1188–1190.

Deshaies, R.J., Sanders, S.L., Feldheim, D.A., and Schekman, R. (1991). Assembly of yeast Sec proteins involved in translocation into the endoplasmic reticulum into a membrane-bound multisubunit complex. Nature *349*, 806–808.

Dreyfuss, G., Choi, Y.D., and Adam, S.A. (1984). Characterization of heterogeneous nuclear RNA-protein complexes in vivo with monoclonal antibodies. Mol. Cell. Biol. *4*, 1104–1114.

Granneman, S., Kudla, G., Petfalski, E., and Tollervey, D. (2009). Identification of protein binding sites on U3 snoRNA and pre-rRNA by UV cross-linking and high-throughput analysis of cDNAs. Proc. Natl. Acad. Sci. USA *106*, 9613–9618.

Guo, H., Ingolia, N.T., Weissman, J.S., and Bartel, D.P. (2010). Mammalian microRNAs predominantly act to decrease target mRNA levels. Nature *466*, 835–840.

Hagan, J.P., Piskounova, E., and Gregory, R.I. (2009). Lin28 recruits the TUTase Zcchc11 to inhibit let-7 maturation in mouse embryonic stem cells. Nat. Struct. Mol. Biol. *16*, 1021–1025.

Hamilton, R.L., Moorehouse, A., Lear, S.R., Wong, J.S., and Erickson, S.K. (1999). A rapid calcium precipitation method of recovering large amounts of highly pure hepatocyte rough endoplasmic reticulum. J. Lipid Res. *40*, 1140–1147.

Heo, I., Joo, C., Cho, J., Ha, M., Han, J., and Kim, V.N. (2008). Lin28 mediates the terminal uridylation of let-7 precursor MicroRNA. Mol. Cell *32*, 276–284.

Heo, I., Joo, C., Kim, Y.K., Ha, M., Yoon, M.J., Cho, J., Yeom, K.H., Han, J., and Kim, V.N. (2009). TUT4 in concert with Lin28 suppresses microRNA biogenesis through pre-microRNA uridylation. Cell *138*, 696–708.

Ingolia, N.T., Ghaemmaghami, S., Newman, J.R., and Weissman, J.S. (2009). Genome-wide analysis in vivo of translation with nucleotide resolution using ribosome profiling. Science *324*, 218–223.

Ingolia, N.T., Lareau, L.F., and Weissman, J.S. (2011). Ribosome profiling of mouse embryonic stem cells reveals the complexity and dynamics of mammalian proteomes. Cell *147*, 789–802.

Kishore, S., Jaskiewicz, L., Burger, L., Hausser, J., Khorshid, M., and Zavolan, M. (2011). A quantitative analysis of CLIP methods for identifying binding sites of RNA-binding proteins. Nat. Methods *8*, 559–564.

Kutay, U., Hartmann, E., and Rapoport, T.A. (1993). A class of membrane proteins with a C-terminal anchor. Trends Cell Biol. *3*, 72–75.

Licatalosi, D.D., and Darnell, R.B. (2010). RNA processing and its regulation: global insights into biological networks. Nat. Rev. Genet. *11*, 75–87.

Licatalosi, D.D., Mele, A., Fak, J.J., Ule, J., Kayikci, M., Chi, S.W., Clark, T.A., Schweitzer, A.C., Blume, J.E., Wang, X., et al. (2008). HITS-CLIP yields genome-wide insights into brain alternative RNA processing. Nature *456*, 464–469.

Loughlin, F.E., Gebert, L.F., Towbin, H., Brunschweiger, A., Hall, J., and Allain, F.H. (2012). Structural basis of pre-let-7 miRNA recognition by the zinc knuckles of pluripotency factor Lin28. Nat. Struct. Mol. Biol. *19*, 84–89.

Mili, S., and Steitz, J.A. (2004). Evidence for reassociation of RNA-binding proteins after cell lysis: implications for the interpretation of immunoprecipitation analyses. RNA *10*, 1692–1694.

Moss, E.G., and Tang, L. (2003). Conservation of the heterochronic regulator Lin-28, its developmental expression and microRNA complementary sites. Dev. Biol. *258*, 432–442.

Moss, E.G., Lee, R.C., and Ambros, V. (1997). The cold shock domain protein LIN-28 controls developmental timing in C. elegans and is regulated by the lin-4 RNA. Cell *88*, 637–646.

Nam, Y., Chen, C., Gregory, R.I., Chou, J.J., and Sliz, P. (2011). Molecular basis for interaction of let-7 microRNAs with Lin28. Cell *147*, 1080–1091.

Newman, M.A., Thomson, J.M., and Hammond, S.M. (2008). Lin-28 interaction with the Let-7 precursor loop mediates regulated microRNA processing. RNA *14*, 1539–1549.

Peng, S., Chen, L.L., Lei, X.X., Yang, L., Lin, H., Carmichael, G.G., and Huang, Y. (2011). Genome-wide studies reveal that Lin28 enhances the translation of genes important for growth and survival of human embryonic stem cells. Stem Cells *29*, 496–504.

Piskounova, E., Polytarchou, C., Thornton, J.E., LaPierre, R.J., Pothoulakis, C., Hagan, J.P., Iliopoulos, D., and Gregory, R.I. (2011). Lin28A and Lin28B inhibit let-7 microRNA biogenesis by distinct mechanisms. Cell *147*, 1066–1079.

Polesskaya, A., Cuvellier, S., Naguibneva, I., Duquet, A., Moss, E.G., and Harel-Bellan, A. (2007). Lin-28 binds IGF-2 mRNA and participates in skeletal myogenesis by increasing translation efficiency. Genes Dev. *21*, 1125–1138.

Qiu, C., Ma, Y., Wang, J., Peng, S., and Huang, Y. (2010). Lin28-mediated post-transcriptional regulation of Oct4 expression in human embryonic stem cells. Nucleic Acids Res. *38*, 1240–1248.

Rybak, A., Fuchs, H., Smirnova, L., Brandt, C., Pohl, E.E., Nitsch, R., and Wulczyn, F.G. (2008). A feedback loop comprising lin-28 and let-7 controls pre-let-7 maturation during neural stem-cell commitment. Nat. Cell Biol. *10*, 987–993.

Suzuki, H., Kamada, N., Ueda, O., Jishage, K., Kurihara, Y., Kurihara, H., Terauchi, Y., Azuma, S., Kadowaki, T., Kodama, T., et al. (1997). Germ-line contribution of embryonic stem cells in chimeric mice: influence of karyotype and in vitro differentiation ability. Exp. Anim. *46*, 17–23.

Thornton, J.E., and Gregory, R.I. (2012). How does Lin28 let-7 control development and disease? Trends Cell Biol. *22*, 474–482.

Ule, J., Jensen, K.B., Ruggiu, M., Mele, A., Ule, A., and Darnell, R.B. (2003). CLIP identifies Nova-regulated RNA networks in the brain. Science *302*, 1212–1215.

Ule, J., Jensen, K., Mele, A., and Darnell, R.B. (2005). CLIP: a method for identifying protein-RNA interaction sites in living cells. Methods *37*, 376–386.

Viswanathan, S.R., Daley, G.Q., and Gregory, R.I. (2008). Selective blockade of microRNA processing by Lin28. Science *320*, 97–100.

Viswanathan, S.R., Powers, J.T., Einhorn, W., Hoshida, Y., Ng, T.L., Toffanin, S., O'Sullivan, M., Lu, J., Phillips, L.A., Lockhart, V.L., et al. (2009). Lin28 promotes transformation and is associated with advanced human malignancies. Nat. Genet. *41*, 843–848.

Wagenmakers, A.J., Reinders, R.J., and van Venrooij, W.J. (1980). Cross-linking of mRNA to proteins by irradiation of intact cells with ultraviolet light. Eur. J. Biochem. *112*, 323–330.

Wu, T.D., and Nacu, S. (2010). Fast and SNP-tolerant detection of complex variants and splicing in short reads. Bioinformatics *26*, 873–881.

Xu, B., and Huang, Y. (2009). Histone H2a mRNA interacts with Lin28 and contains a Lin28-dependent posttranscriptional regulatory element. Nucleic Acids Res. *37*, 4256–4263.

Xu, B., Zhang, K., and Huang, Y. (2009). Lin28 modulates cell growth and associates with a subset of cell cycle regulator mRNAs in mouse embryonic stem cells. RNA *15*, 357–361.

Yu, J., Vodyanik, M.A., Smuga-Otto, K., Antosiewicz-Bourget, J., Frane, J.L., Tian, S., Nie, J., Jonsdottir, G.A., Ruotti, V., Stewart, R., et al. (2007). Induced pluripotent stem cell lines derived from human somatic cells. Science *318*, 1917–1920.

Zhang, C., and Darnell, R.B. (2011). Mapping in vivo protein-RNA interactions at single-nucleotide resolution from HITS-CLIP data. Nat. Biotechnol. *29*, 607–614.

Zhu, H., Shah, S., Shyh-Chang, N., Shinoda, G., Einhorn, W.S., Viswanathan, S.R., Takeuchi, A., Grasemann, C., Rinn, J.L., Lopez, M.F., et al. (2010). Lin28a transgenic mice manifest size and puberty phenotypes identified in human genetic association studies. Nat. Genet. *42*, 626–630.

Zhu, H., Shyh-Chang, N., Segrè, A.V., Shinoda, G., Shah, S.P., Einhorn, W.S., Takeuchi, A., Engreitz, J.M., Hagan, J.P., Kharas, M.G., et al; DIAGRAM Consortium; MAGIC Investigators. (2011). The Lin28/let-7 axis regulates glucose metabolism. Cell *147*, 81–94.